J. Min. Metall. Sect. B-Metall. 55 (1) B (2019) 21 - 29

Journal of Mining and Metallurgy, Section B: Metallurgy

THERMODYNAMIC MODELLING OF THE LEAD SINTERING ROASTING PROCESS

T. Rojas Sánchez [a], A. Romero Serrano [a*], A. Hernandez Ramírez [a], J. Lopez Rodríguez [a], I. Almaguer Guzmán [b], R. Benavides Pérez [b], M. Flores Favela [b]

[a*] Instituto Politecnico Nacional-ESIQIE, Mexico City, Mexico
[b] Servicios Administrativos Peñoles S.A de C.V., Torreón Coahuila, Mexico

(Received 18 September 2018; accepted 03 January 2019)

Abstract

This work proposes a simulation strategy of the lead sintering process assuming that it takes place in a horizontally moving packed bed with transverse air flow. Some local chemical reactions occur at rates that depend on the temperature, and chemical species formed in one volume stage will flow for further reaction in other stages. To simulate this process, the model reactor is divided into a number of sequential stages. Condensed species flow horizontally, and gaseous species leave each stage vertically. The compositions and temperatures of the species are calculated considering that the local thermodynamic equilibrium is reached in each stage without external heat transfer, apart from the gas flow, before moving on to the next stage. The model calculates the temperature profile along the sintering machine, the compositions of the sinter and the exhaust gas. The results of the proposed model were compared with sinter pot experimental trials and a reasonably good agreement was obtained. This model can be used to optimize the operating conditions of the lead sintering process.

Keywords: *Lead concentrate; Sintering process; Thermodynamic simulation*

1. Introduction

Sinter-blast furnace route is still one of the most important smelting technologies employed to produce lead. The sinter-roasting of lead concentrate is usually carried out in a Dwight-Lloyd sintering machine which consists of an endless chain of steel pallets, each made from a frame fitted with steel bars to form a grate [1]. The charge materials contain pellets comprising three constituents: the concentrate mixture, the fluxes (silica and calcium carbonates) and recycled sinter material. The objective of this process is to attain a temperature wave to pass through the bed in such a way that a zone of incipient or partial fusion passes through the bed to agglomerate the material to a porous lumpy product.

The sintering process includes ignition and autogenous stages, as shown in Figure 1. A thin layer of charge material, about 4 to 8 cm thick, is deposited on the grate, then ignited with gas burners to initiate the exothermic sulphide oxidation reaction. The airflow direction during ignition is down. The remainder of the pellet mixture is then discharged onto this "ignition" layer, to form a pellet bed about 30 to 50 cm deep. The air blown up through the bottom of the grid ensures propagation of the reaction through the bed in the autogenous stage.

The primary sintering reaction is:

$$2PbS + 3O_2 = 2PbO + 2SO_2 \quad (1)$$

Other side reactions that can occur are:

$$2PbS + 3O_2 = 2PbO + 2SO_2 \quad (2)$$

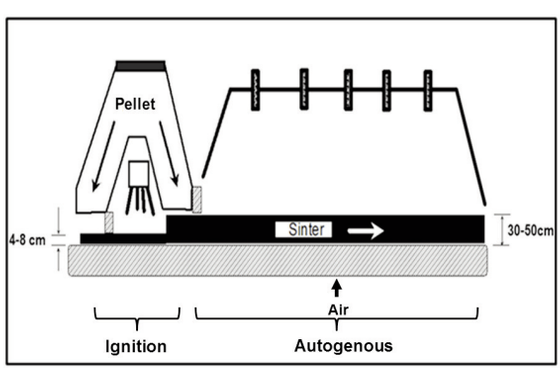

Figure 1. *Schematic representation of the sinter machine*

**Corresponding author: romeroipn@hotmail.com*

DOI:10.2298/JMMB180918006R

$$PbS + 2\,O_2 = PbSO_4 \quad (3)$$

$$PbS + PbSO_4 = 2Pb + 2SO_2 \quad (4)$$

$$PbS + 2PbO = 3\,Pb + SO_2 \quad (5)$$

The main parameters which define the quality of sinter are the peak bed temperature, permeability, degradation behaviour, softening characteristics and its sulphur content. Sinclair [2] has reported that gas permeability of the bed can be reduced by the effect of moisture evaporation, the entrainment of fine particles and the formation of liquid phases.

The microstructure of sinter is quite complex but can be considered as a matrix of crystalline phases and a glassy phase composed of lead silicate glass [2]. The crystalline phases are melilite minerals of which hardystonite ($Ca_2ZnSi_2O_7$) is one particular form, and franklinite ($ZnFe_2O_4$) [3]. The required structure of sinter is obtained at a high temperature and, to produce it, it is important that peak bed temperature is above 1200°C. Sinters with low quality contains excessive lead silicate phases without the tight matrix of the intergrown crystal phases to provide structural support. The melting temperature of the mineralogical species of the system is important for determining the softening of the sinter structure. For example, lead silicates have low melting point, between 600°C and 800°C. The melting point is raised by the addition of CaO to increase the $CaO:SiO_2$ ratio. Finally, the residual amount of sulphur in sinter is important for obtaining a suitable sinter structure as well as meeting the maximum limits of sulphur for the blast furnace, and it is generally less than two percent.

Despite accumulated knowledge and experience, the continuous and optimized control of the performance of the lead sintering roasting process still remains a difficult task. Several numerical approaches have been proposed in the literature to simulate the behaviour of this process. However, there is no efficient method for evaluating quickly optimal operating parameters of a sintering roasting process as a function of the lead concentrates composition.

Bellot et al. [4] developed a model for the sintering of zinc sulphides ores by dividing the sinter bed into four zones and calculated the transient temperatures and compositions of the solids and gases in the bed. Siemon et al. [5] used a computer program to improve the sinter composition in a lead/zinc sinter plant by the use of charge calculation which included as a target the theoretical peak bed temperature. Xu et al. [6] and Gui et al. [7] described the modelling and state optimization of the permeability and heat states of the lead-zinc sintering process. Zhou et al. [8] modelled the iron ore sintering process taking into account the flame front, heat transfer, and the physicochemical reactions. Saiz and Posada [9] developed a model in accordance with estimation and control theories of stochastic processes.

Zhang et al. [10] simulated the sintering process of iron ore by an unsteady two-dimensional mathematical model, which incorporated the significant physical phenomena and chemical reactions; sinter pot tests were also carried out. Wang et al. [11] established a research route with sinter pot trials to characterize the evolution of the flame front and the phase chemistry along the bed height of sintering. Zhao et al. [12] reported the evaluation model of iron ore properties based on the high-temperature characteristic numbers by employing fuzzy mathematics. With the constraint of sinter properties and the raw materials, they built the ore blending model, whose target was to obtain the best sinter properties at the lowest cost. Ding et al. [13] proposed a temperature model to explain the effect of the airflow rate on the sinter bed temperature. They proposed the application of an algorithm based on the optimization of airflow rate as the control strategy for the sintering process. Wang et al. [14] reported the evolution of the flame front and the mineral phases along the bed height of sintering.

The present article describes a model of the lead sulphide concentrate sinter-roasting operation assuming that it takes place in a horizontally moving packed bed with transverse air flow. To simulate this process, the model reactor is divided into a number of sequential stages. The compositions and temperatures of the flowing chemical species are calculated assuming that the local equilibrium is reached in each stage without external heat transfer (apart from the gas flow) before the chemical species moves on to the next horizontal stage. The effect of the softening of the material and porosity were not considered in this model.

The results of the model are the temperature profile along the sintering machine, the mineralogical species, and composition contained in the sinter as well as the chemical composition of the exhaust gas. Sinter pot trials were carried out to obtain data to compare with the model's predicted results, specifically in the areas of the maximum temperature and the thermal profile at different regions of the sintering bed.

2. Computational Modelling

2.1 Steady-State Calculation

The process takes place in a horizontally moving packing bed. Various local chemical reactions will occur at rates that are dependent on the temperature. The species formed in one volume stage will flow for further reaction in other stages or will form part of the products leaving the reactor. To simulate this process, the reactor is divided into a number of sequential stages. Gaseous and condensed species leave a given

stage to react in the neighbouring stages. All the solid or liquid species produced in a stage move to the next adjacent horizontal stage whereas gaseous products leave each stage vertically.

The solution technique is one of repetitive substitution, taking into consideration the stages one by one, and eventually reaching a steady state condition characterized by a total balance in the material and the enthalpy inputs and outputs. Figure 2 shows the reactor structure schematically for the modelling of the sintering machine. The sinter bed is divided vertically into five layers, where the 1st layer is close to the sintering strand and the 5th layer is at the top of the sinter bed. In order to calculate the amounts and temperatures of the flowing species, it is assumed that the chemical reactions proceed to completion at each stage.

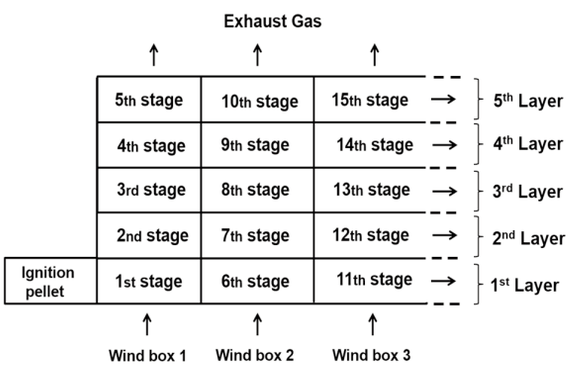

Figure 2. *Reactor structure for the modelling of the sinter machine*

The reactions in each volume segment result in a multiphase system consisting of a gas phase and condensed pure species. The species considered are as follows:

• Gas phase: N_2, O_2, NO, NO_2, CH_4, C_2H_6, C_3H_8, COS, CO, CO_2, H_2, H_2O, HS, S_2, SO, SO_2, SO_3, Pb, PbS, PbO, Zn, ZnS, HCN, CuO.

• Condensed pure species: C, CaO, $CaCO_3$, $Ca_2ZnSi_2O_7$, $CaSO_4$, $CaSiO_3$, Pb, PbO, PbO_2, Pb_3O_4, $PbCO_3$, $PbSO_4$, Pb_3SO_6, $Pb_4S_2O_7$, Pb_2SO_5, $PbSiO_3$, Pb_2SiO_4, Pb_4SiO_6, ZnS, ZnO, $PbZnSiO_4$, $ZnFe_2O_4$, Zn_2SiO_4, FeO, FeS, Fe_2O_3, Fe_3O_4, FeS_2, SiO_2, H_2O, $Cu_2Fe_2O_4$, $CuFeS_2$, $Pb_3Ca_2Si_3O_{11}$, $PbCa_2Si_3O_9$, $Pb_2FeSi_2O_7$, CuO, Cu_2S.

All the thermodynamic data of the species considered in the equilibrium calculations were taken from the compilation of Barin [15]. It is worth noting that melilite refers to a group of minerals with chemically similar composition according to the formula $(Ca,Na)_2(Mg,Zn,Al)(Si,Al)_2O_7$. However, in the lead-zinc concentrates considered in this work, hardystonite ($Ca_2ZnSi_2O_7$) is the main component. Similarly, franklinite ($ZnFe_2O_4$) is considered as the main component in the spinel group. No solid solutions were considered in this thermodynamic approach.

The chemical equilibrium calculations in each stage were carried out by the global minimization of the Gibbs energy, which can be uniquely defined with respect to temperature, pressure, and composition [16]. The model considers an enthalpy-regulated stage where the constant reaction temperature is determined by the chemical and thermal equilibria that are established.

2.2 General Aspects of the Gibbs Energy Minimization

The principal aim of the chemical equilibrium calculations is to determine the equilibrium composition of the species of the system under specific conditions, such as temperature, pressure, and composition. Smith and Missen [17] classified the algorithms for chemical reaction equilibrium calculation into two main categories, the stoichiometric and the non-stoichiometric methods. In the stoichiometric methods, linearly independent reactions of known stoichiometric coefficients, and the equilibrium constants are used in the calculations. This method must take into account the reactions that takes place along the process such as oxidation reactions, decomposition reactions of carbonates, and melting and solidification.

In the non-stoichiometric methods, the Gibbs energy function is minimised in terms of composition, temperature, and pressure. While in the stoichiometric method the independent reactions should be defined, in the non-stoichiometric method the necessary information is only the number of components and their Gibbs energies. In the non-stoichiometric method, the path followed to change the system from an initial state to a final state is not important since the Gibbs energy is a state function. Gibbs energy is a property of a system that has a value that depends upon the current condition of the system, and not upon the process of the system's attainment of that condition.

Eriksson and Rosen [18] showed that the total Gibbs energy of a system, which has to be minimized for a given temperature, pressure, and composition to establish equilibrium, is often represented as

$$G = \sum_i n_i g_i = \sum_i \mathbf{n}_i \left(g_i^o + RT \ln a_i \right) \quad (6)$$

Where n_i denotes the amounts of the species, g_i the chemical potentials, ai the activities, R the gas constant, and T the absolute temperature. If we consider that the system contains only an ideal gas phase and pure solid or liquid species, Eq. (6) can be expressed as:

$$G = \sum_{i,gas} n_i \left(g_i^o + RT \ln \frac{p_i}{p_i^o} \right) + \sum_{j,pure} n_j \, g_j^o \qquad (7)$$

where p_i is the partial pressure of the species i in the gas phase and p_i^o is the pressure of ideal gas i in its standard state (1 bar). The minimization of Eq. (7) at constant temperature and pressure is achieved with the constraints imposed by the mass balance equations. In terms of the r independent system components, these mass balance equations may be written as:

$$\sum_q \sum_i n_i^q m_{ij}^q = b_j \quad (j = 1, 2, \ldots, r) \qquad (8)$$

where n_i^q is the amount of the ith species of phase q, m_{ij}^q is a coefficient of the stoichiometry matrix composed of the species of phase q, and b_j is the total amount of the jth system component.

2.3 Simulation algorithm

The autogenous section of the sintering machine was divided into fifty stages, ten horizontal by five vertical, in the reactor to model the process. In each stage, the local temperature and the chemical species in equilibrium had to be calculated. The local temperature can be calculated assuming that the exothermic heat of reaction plus the heat supplied by incoming gas is absorbed by the products and the outgoing gas so as to give a zero change in enthalpy ($\Delta H=0$). There can be heat loss by convection and radiation mainly from the top of the sinter bed, but the model does not consider this effect; we assume that the heat loss is negligible since the lead sinter machine is a closed system.

The algorithm to calculate the temperature in each stage is shown in Figure 3. In the first step of the iteration, the change in enthalpy (ΔH) of the process is calculated at an assumed temperature between the minimum and the maximum temperatures (T_{min} and T_{max}). If ΔH is positive, the equilibrium temperature is lower than that which was assumed (T_1), and the temperature in the next iteration is at the middle of T_{min} and T_1. If ΔH is negative, as it is the case in the example of Figure 3, the equilibrium temperature is higher than T_1, and the temperature in the second iteration (T_2) is taken as at the middle of T_1 and T_{max}. In this example, the equilibrium temperature is again between T_2 and T_{max}, so the temperature at the middle of T_2 and T_{max} is tested in the third iteration (T_3). This procedure is repeated until the tested temperature fulfils with a stopping criterion, $\Delta H<0.1$ J. This method enables us to calculate the equilibrium temperature of each stage in less than ten iterations.

Figure 4 illustrates how the condensed species produced at one stage move horizontally to the next stage and react with the phase gas produced at the previous stage. Let us assume that the solid or liquid chemical species that are produced in the 8th stage at 681°C move to the 13th stage and there they react with the gas phase coming from 12th stage at 852°C. After reaching the equilibrium the condensed species move to 18th stage at 968°C, whereas the gas phase move to 14th stage also at 968°C.

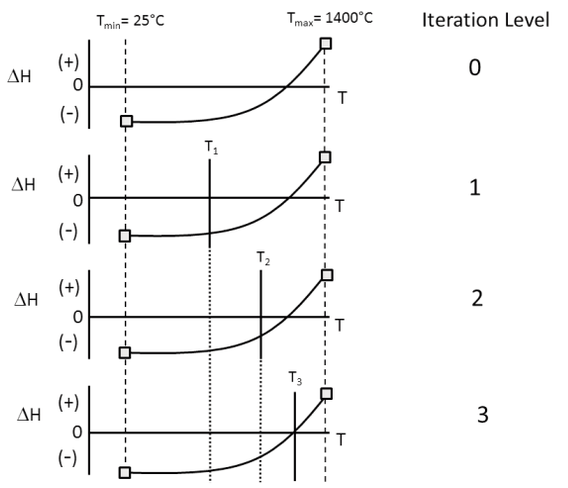

Figure 3. *Illustration of the steps to estimate the equilibrium temperature in each stage*

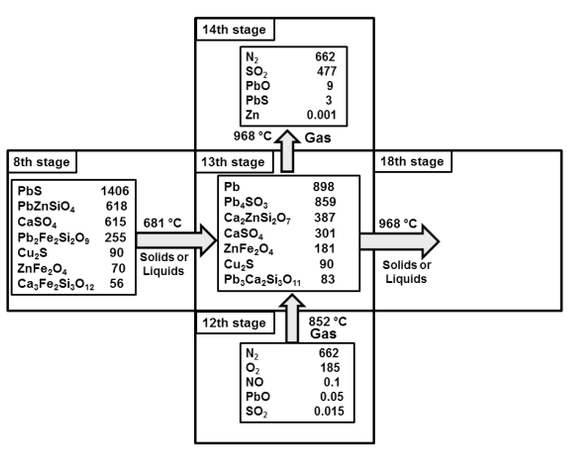

Figure 4. *Example of the species reacting at a given stage (mass in kg)*

3. Experimental Procedure

3.1. Experimental Pilot-Scale Plant

Experiments have been carried out in this work on a sinter pot, and the results have been compared with the results yielded by the model. These trials were aimed at providing an understanding of the effect of sinter composition on the temperature profile and that the maximum temperature of the sinter bed as a

function of time. Table 1 shows the composition of the main mineralogical species of the lead concentrate, the recycled sinter, the obtained pellets, and the sulphide content. It is worth noting that these pellets were formed by mixture comprising 40% of lead concentrate and 60% of recycled sinter. In the process of sintering of lead sulphide concentrates, to achieve the necessary peak bed temperature, the sulphur content in the form of sulphide should be 6% to 7% of the charge. Since sulphur content in the sulphide form in lead concentrates normally ranges from 15% to 25%, it needs to be diluted before sintering. Usually, this dilution is achieved by the addition of recycled sinter.

The sinter pot has a cross-sectional area 730 cm^2 and height 36 cm. Four type K thermocouples were mounted at 3, 15, 22 and 32 cm from the upper end of the reactor to measure the temperature. The pellets were granulated and then were put into the reactor. The particle size analysis of the pellet showed that 88 wt% was between 0.125 and 0.95 cm. The upper surface of the formed bed was ignited for 3 min using a gas burner with an airflow of 40 Nm^3/h (548 Nm^3/h per m^2 of the cross-sectional area). After the ignition, the rate of blowing air was increased to 70 Nm^3/h (959 Nm^3/h per m^2 of the cross-sectional area), and that rate was maintained until the end of sintering. The bed temperature was continuously monitored during sintering. The airflow direction in the sinter pot trials was down; however, in a sintering machine, the down-drafted action tends to compress the bed against the grate and reduce its permeability. It is also found that in the down-drafted sintering significant amount of metallic lead tends to drain down onto the grate and causes blockages.

To simulate the sinter process in the reactor, the sinter pot was divided into six stages of 6 cm each. The temperature in the middle of each stage was calculated at 3, 15, 21 and 33 cm from the upper side, which nearly coincide with the position of the thermocouples in the experimental array. It is worth mentioning that although the model is based on thermodynamic equilibrium, there is a time effect due to the fixed flow rate of air to the system, which limits the oxygen available at each stage. Thus, the extent of reaction between the gas phase and the condensed species for a given period was determined by the oxygen supply in that time period. Hence, time is an important parameter.

3.2 Experimental pilot-scale plant temperature profiles

Figure 5 shows the calculated and the experimental temperature profiles in the sinter pot in terms of the processing time. Once ignited, the combustion is sustained by sulphur-oxygen reactions.

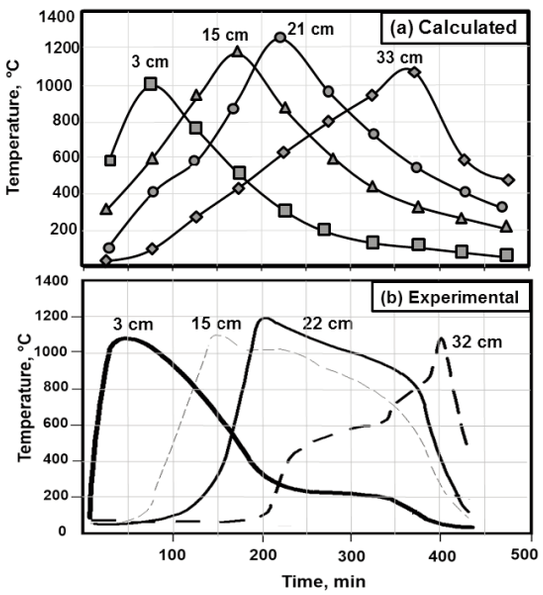

Figure 5. *Measured and calculated temperature in the sinter pot trial. The curves represent the temperature profiles at the given distance from the upper end of the sinter pot*

Table 1. *Mineralogical composition of the materials for the sinter pot trials*

Chemical Species	Lead ore concentrate wt. %	Recycle Sinter wt. %	Final Pellet wt. %
PbS	29.59	4.81	14.72
$PbSO_4$	0	22.05	13.23
$Ca_2ZnSi_2O_7$	0	17.32	10.39
Pb_4SiO_6	0	18.73	11.24
$CaSO_4$	0	12.55	7.53
H_2O	6.33	7.75	7.18
$CaCO_3$	3.66	0.26	1.62
ZnS	11.37	0.2	4.67
Fe_3O_4	0	4.15	2.49
$CuFeS_2$	26.38	1.8	11.63
FeS_2	19.88	0.63	8.33
CuO	0	3.4	2.04
PbO	0	4.08	2.45
SiO_2	2.79	0.19	1.23
Pb	0	2.08	1.25
% Sulphur as sulphide of the total mass	27.02	1.68	12.03
% Sulphur as sulphate of the total mass	0	5.28	3.17

As the combustion zone proceeds downward, combustion thickness and maximum temperature increase. It is observed that the calculated and experimental temperature results are in good agreement. However, the slight differences that are observed can be due to the fact that the temperature in the sinter pot is difficult to measure because it depends strongly on local airflow rate around the thermocouple tip and its distance from particles undergoing exothermic or endothermic reactions, as was observed by Loo and Dukino [19]. Mežibrický and Fröhlichová [20] carried out sinter trials of iron ore and obtained similar temperature profiles to those of Figure 5. Figure 6 shows a comparison between the evaluated and the experimental temperatures at different points from the top of the sinter pot.

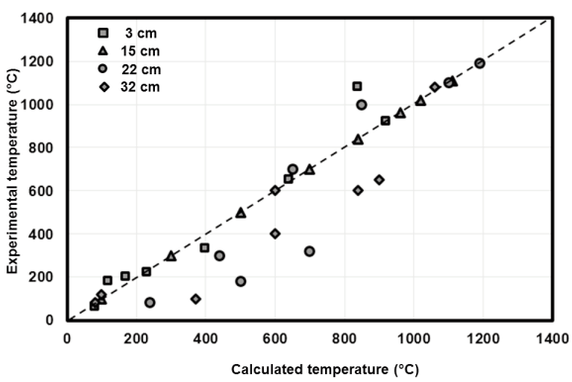

Figure 6. *Comparison of the calculated and experimental temperatures at given distance from the top of the sinter pot*

The experimental temperature-time profile has a shape characterized by a very steep temperature gradient at the leading edge and a gentler downward sloping section towards the trailing edge. Loo and Dukino [21] proposed that a solid, liquid and gas mixture was generated at the flame front and it encountered a uniform bed, which caused the steep rise in temperature at the leading edge. However, at the trailing edge, the flow channels were uneven in size and distributed randomly, which caused the cooling rate at the trailing edge to be slower as compared to the heating rate at the leading edge. Thus, the bed structure differences affect the heating and cooling processes at the two edges.

4. Simulation of the Lead Sintering Roasting Process

The described thermodynamic algorithm has been implemented to simulate the thermal behaviour of a sintering machine with a 1.5 m of ignition zone and 40 m length of autogenous zone, which may process about 240 ton/h of lead concentrate pellets. As a case study, this model is used in the simulation of the conventional lead sintering-roasting process of two types of pellets (Pellets A and B) with the compositions shown in Tables 2 and 3, respectively. These Tables show the composition of the lead concentrates, the recycled sinters, the obtained pellets and their sulphide contents. These cases are considered to estimate the effect of the sulphur content on the temperature distribution in the bed sinter, on the chemical composition of the final sinter, and the SO_2 content of the exhaust gas.

The phases of samples shown in Tables 2 and 3 were identified using XRD Bruker D8 Focus with Cu Kα (λ=1.5406 Å). The microstructural analysis was performed using scanning electron microscopy coupled with an energy-dispersive spectra analyser (FEI Quanta 600, EDAX EDS) and GENESIS-MLA software (Mineral Liberation Analysis) to determine the compositions of each phase.

4.1. Sintering temperature results

Lead sinter plant simulations were carried out with the actual process parameters. The speed of the sinter machine was maintained at 100 cm/min. Ten wind

Table 2. *Mineralogical composition of the materials used to obtain pellet A*

Chemical Species	Lead ore concentrate wt. %	Recycle Sinter wt. %	Final Pellet wt. %
PbS	75.92	4.81	33.25
$PbSO_4$	0	22.05	13.23
$Ca_2ZnSi_2O_7$	0	17.32	10.39
Pb_4SiO_6	0	18.73	11.24
$CaSO_4$	0	12.55	7.53
H_2O	5.53	7.75	6.86
$CaCO_3$	7.76	0.26	3.26
ZnS	7.02	0.2	2.93
Fe_3O_4	0	4.15	2.49
$CuFeS_2$	2.11	1.8	1.91
FeS_2	0.63	0.63	0.63
CuO	0	3.4	2.04
PbO	0	4.08	2.45
SiO_2	1.03	0.19	0.52
Pb	0	2.08	1.25
% Sulphur as sulphide of the total mass	13.56	1.68	6.42
% Sulphur as sulphate of the total mass	0	5.28	3.17

boxes were assumed to blow air in the sinter machine at the autogenous stage. The temperature profiles obtained for the trial with pellet A are shown in Figure 7. This figure shows five curves since the bed was divided vertically in five layers. The curve of the 1st layer corresponds to the temperature profile in the bed close to the sintering strand, whereas the curve of the 5th layer represents the temperature profile at the bed in contact with the atmosphere in the sintering machine. It can be seen that in this trial the peak bed temperature was about 1217°C, between 20 and 24 m from the main hopper, above the 6th wind box. In this case, the temperature at the upper side of the bed diminished rapidly after the peak temperature and remained above 560 ºC until the end of the sinter bed.

Results of the calculated temperatures for the second trial (pellet B) are shown in Figure 8. A peak temperature about 1306°C at the top of the bed was achieved between 32 and 36 m from the main hopper. The temperature at the upper side of the bed dropped and remained above 1000 ºC until the end of the sinter bed. The higher peak temperature obtained with pellet B is due to the higher sulphide content of this material.

Table 3. *Mineralogical composition of the materials used to obtain pellet B*

Chemical Species	Lead ore concentrate wt. %	Recycle Sinter wt. %	Final Pellet wt. %
PbS	41.97	4.81	19.67
$PbSO_4$	0	22.05	13.23
$Ca_2ZnSi_2O_7$	0	17.32	10.39
Pb_4SiO_6	0	18.73	11.24
$CaSO_4$	0	12.55	7.53
H_2O	6.22	7.75	7.14
$CaCO_3$	5.64	0.26	2.41
ZnS	7.9	0.2	3.28
Fe_3O_4	0	4.15	2.49
$CuFeS_2$	26.71	1.8	11.76
FeS_2	8.05	0.63	3.6
CuO	0	3.4	2.04
PbO	0	4.08	2.45
SiO_2	3.51	0.19	1.52
Pb	0	2.08	1.25
% Sulphur as sulphide of the total mass	21.86	1.68	9.75
% Sulphur as sulphate of the total mass	0	5.28	3.17

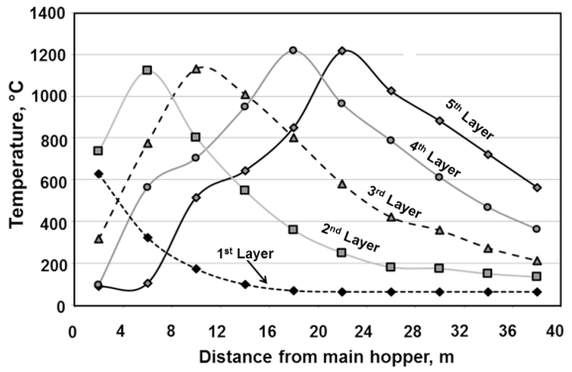

Figure 7. *Bed temperature profiles against distance, obtained with pellet A*

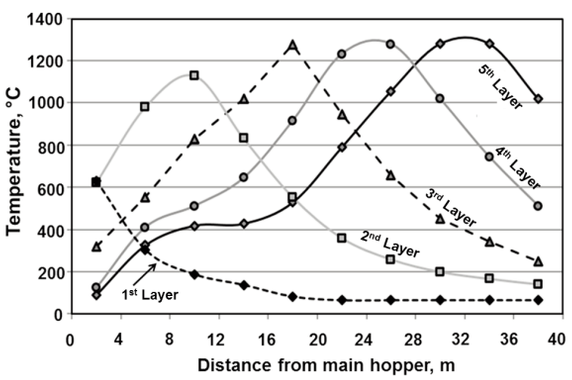

Figure 8. *Bed temperature profiles against distance, obtained with pellet B*

4.2 Sinter composition

Sinclair [2] and Zhao [22] have shown that the mechanical behaviour of the sinter in the blast furnace process depended directly on its microstructure. It was found that in the lead sinter samples melilite [2(Ca,Pb)O(Zn,Fe)O(2SiO$_2$)], spinel [(Zn,Fe,Mg)O(Fe$_2$O$_3$)], lead oxide (PbO) and glass are found to be the common species. Also, some other species such as Pb-Zn silicate ($PbZnSiO_4$), Pb-Ca silicate ($Pb_3Ca_2Si_3O_{11}$), lead sulphide (PbS), calcium sulphates (Ca_2SO_5 and Ca_3SO_6), silica (SiO_2) and Pb metal are also obtained in lead sinters. Melilite and spinel are expected species in the final sinter because they form a framework which supports the sinter lump at high temperature in the lead blast furnace.

The chemical species of the final sinter calculated by the model were grouped in lead oxides, and lead silicates, lead sulphates and lead sulphides, all of them calculated in terms of total lead content. The results of the sinter composition obtained with pellets A and B are shown in Table 4, where the melilite and franklinite phases are also included. These results show that in sinter A, produced at relatively low

temperatures in the sinter bed, oxides, silicates, and sulphates of lead, together with low amounts of melilite and franklinite were obtained. On the other hand, in sinter B, produced at high temperatures, high amounts of melilite, franklinite and oxide and silicates of lead together with a negligible amount of lead sulphates were obtained.

Figure 9 shows the phases of sinters A and B, produced industrially and observed with scanning microscopy. The SEM-EDS results show that the white phase corresponds to lead oxides (O), whereas the grey matrix are the calcium and lead silicates (L). The dark, angular crystals (F) are franklinite and the elongated dark crystals are melilite. It is also observed that sinter A contains a higher amount of lead sulphates (S).

Table 4. *Compositions in terms of types of compounds of the sinter produced by pellets A and B (wt. %)*

Chemical Species	Sinter A	Sinter B
% Pb as oxides and silicates[(a)]	83.43	99.74
% Pb as sulphates[(a)]	16.57	0.26
% Pb as sulphides[(a)]	0	0
% Melilite[(b)]	7.89	14.93
% Franklinite[(b)]	5.35	16.51

(a) Calculated in terms of total Pb
(b) Calculated in terms of total sinter

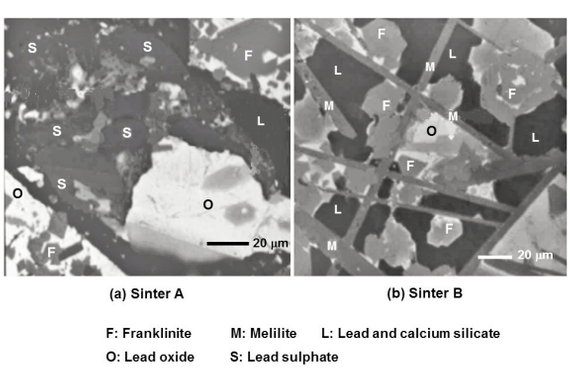

Figure 9. *Microstructures obtained in sinter A and B*

4.3 SO_2 content in the exhaust gases

The model predicts the exhaust gas composition above the bed and along the sintering strand. Figure 10 shows the calculated SO_2 contents in the exhaust gas for sinters A and B. It is evident that the higher sulphur content in pellet B produced a higher amount of SO_2 and the concentration profile had a wide spread. The disadvantage of high sulphide content in the pellet was that SO_2 was still being produced at the end of the strand, which may cause environmental problems.

There is a reasonably good agreement between sinter pot trials and calculated results obtained by the thermodynamic-based model in the areas of bed temperature profiles and maximum temperatures, without the necessity of adding adjusting parameters. The agreement is close, even though the model does not consider some phenomena explicitly in sintering such as the permeability state of the process, and gas flow and pressure relationship in the bed. This model can be used as the first approach to designing the pellet composition to obtain a sinter with the required chemical characteristics in the lead blast furnace.

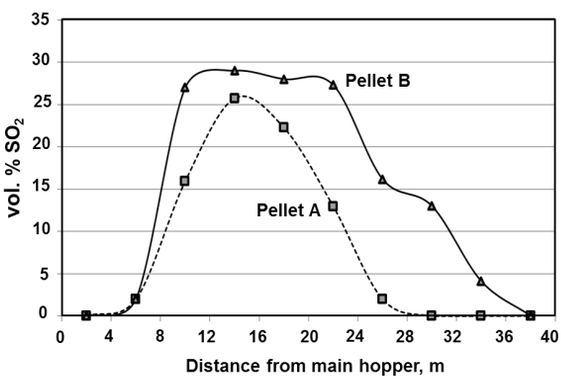

Figure 10. *Predicted SO_2 content in the exhaust gas against distance, obtained with pellets A and B*

Conclusions

A thermodynamic-based model was developed for evaluating the operating parameters for the lead sintering process. A global simulation strategy of the lead sintering process, assuming that it takes place in a horizontally moving packed bed with transverse air flow, was devised. The results of the model are the projection of the temperature profile along the sintering machine, the exhaust gas composition and the mineralogical species contained in the sinter.

In this study, the results from the model were compared with the experimental results from sinter pot tests. Results indicate that the model can simulate the lead concentrate sintering process with a reasonably close correlation between the predicted and the measured temperatures and the flame front profiles.

The operating conditions and the predicted output stream properties calculated by the proposed thermodynamic simulation strategy can be used to design pellet compositions to produce sinters with the optimal chemical properties.

Acknowledgements

The authors wish to thank the company SAPSA and the Institutions CONACyT, SNI, COFAA and IPN for the support of this research.

References

[1] F. Habashi, Handbook of Extractive Metallurgy. Primary metals, secondary metals, light metals. New York, Wiley-VCH, 1997.

[2] R. Sinclair, The Extractive Metallurgy of Lead. Carlton Victoria, Australia. The Australian Institute of Mining and Metallurgy, 2009.

[3] B. Zhao, B. Errington, E. Jak, and P. Hayes. Int. Symposium on Lead and Zinc Processing. Lead and Zinc 2008. p. 133-145.

[4] J. P. Bellot, F. Patisson and D. Ablitzer, Metall. Trans. B, 24B (1993) 27-38.

[5] J. R. Siemon, E. Kowalczyk, D. P. Fitzgibbons and W. Baguley, Minerals Engineering, 4 (1991) 63-78.

[6] C. Xu, M. Wu and J. She, Proc. 6th World Congress on Intelligent Control and Automation, Dalian, China. 2006, p. 1861-1865.

[7] W-H. Gui, C. H. Yang and J. Teng, Int. J. Autom. Comput. 4 (2) (2007) 135-140. DOI: 10.1007/s11633-007-0135-z.

[8] H. Zhou, J. P. Zhao, C. E. Loo, B. G. Ellis and K. F. Cen, ISIJ Int., 52 (9) (2012) 1550-1558.

[9] J. Saiz, M. A. Posada, ISIJ Int., 53 (2013) 1658-1664.

[10] B. Zhang, J. Zhou, M. Li and Y.Li. ISIJ Int., 58 (1) (2018) 17-24.

[11] Y. Wang, J. Zhang, Z. Liu, Y. Zhang, D. Liu and Yi-ran Liu. Int. J. Min., Metall. and Mater. 24 (10) (2017), 1087-1095.

[12] Y. Zhao, K. Wu, W. Zhan, C. Zhu and Xiao-dong Du. TMS 2018: 9th International Symposium on High-Temperature Metallurgical Processing, p 805-815.

[13] Z. Ding, Q. Sun, S. Liu and Z. Chen. Proceedings of 2017 Chinese Intelligent Systems Conference, p 277-285.

[14] Y. Wang, J. Zhang, Z. Liu, Y. Zhang, D. Liu, and Y. Liu. Int J Miner Metall Mater. 24 (10) (2017), 1087-1095.

[15] I. Barin, Thermochemical Data of Pure Substances. Berlin, Wiley, 1989.

[16] Y. Lwin, Int. J. Engng. Ed., 16 (4) (2000), 335-339.

[17] W. R. Smith and R. W. Missen, Chemical Reaction Equilibrium Analysis: Theory and Algorithms. John Wiley and Sons. New York, 1982.

[18] G. Eriksson and E. Rosen, Chemica Scripta, 4 (1973) 193-194.

[19] C. E. Loo and R. D. Dukino, Miner. Process. Extr. Metall., 123 (4) (2014) 191-196.

[20] R. Mežibrický and M. Fröhlichová, J. Min. Metall. Sect. B-Metall. 54 (1) B (2018) 9-20.

[21] C. E. Loo and R. D. Dukino, Miner. Process. Extr. Metall., 123 (4) (2014) 197-203.

[22] B. Zhao, Sintering Applications. Chapter 8 Lead and Zinc Sintering. Edited by Burcu Ertu, 2013, p. 165-200.

TERMODINAMIČKO MODELOVANJE POSTUPKA SINTEROVANJA I PRŽENJA OLOVA

T. Rojas Sánchez [a], A. Romero Serrano [a*], A. Hernandez Ramírez [a], J. Lopez Rodríguez [a], I. Almaguer Guzmán [b], R. Benavides Pérez [b], M. Flores Favela [b]

[a*] Nacionalni politehnički institut -ESIQIE, Meksiko
[b] Administrativne usluge Penjoles S.A de C.V., Meksiko

Apstrakt

U ovom radu je predstavljena strategija simulacije postupka sinterovanja koncentrata olova koja se odvija u horizontalno postavljenom ležištu sa dijagonalnim protokom vazduha. Neke od lokalnih hemijskih reakcija se odvijaju brzinama koje zavise od temperature, a hemijski proizvodi nastali tokom jedne zapreminske faze će preći u sledeću fazu gde će se odvijati naredna reakcija. Da bi bilo moguće simulirati ovaj postupak, model reaktora je podeljen na određeni broj uzastopnih faza. Kondenzovani proizvodi protiču horizontalno, dok gasoviti proizvodi napuštaju svaku fazu vertikalno. Sastav i temperature proizvoda se izračunavaju na osnovu trenutne termodinamičke ravnoteže koje se dostiže u svakoj fazi bez spoljnog prenošenja toplote, ne uzimajući u obzir protok gasa, pre prelaska u narednu fazu. Model izračunava temperaturni profil duž mašine za sinterovanje, sastav proizvoda nastalih sinterovanjem, kao i sastav izduvnih gasova. Dobijeni rezultati su upoređeni sa rezultatima eksperimenata i oni se u priličnoj meri poklapaju. Ovaj model se može koristiti za optimizaciju uslova u kojima se vrši postupak sinterovanja koncentrata olova.

Ključne reči: *Koncentrat olova; Postupak sinterovanja; Termodinamička simulacija.*